ADVANCED ENERGY MATERIALS

Supporting Information

for *Adv. Energy Mater.*, DOI 10.1002/aenm.202300394

Dispersive Charge Transfer State Electroluminescence in Organic Solar Cells

*Raju Lampande, Adrian Pizano, Manting Gui, Robert Cawthorn, Barry P. Rand and Noel C. Giebink**

Supporting Information

Dispersive charge transfer state electroluminescence in organic solar cells

*Raju Lampande, Adrian Pizano, Manting Gui, Robert C. Cawthorn, Barry P. Rand, and Noel C. Giebink**

S1. CT MELS transfer functions including re-dissociation and reverse intersystem crossing

The possibility of CT state re-dissociation can be accounted for in the MELS transfer function by including an Onsager-Braun[52] style dissociation rate, k_d, in Equation (1):

$$\frac{dn}{dt} = \frac{dp}{dt} = \frac{J_\mathrm{r}}{qa} - \gamma np + k_\mathrm{d} s \,, \tag{S1a}$$

$$\frac{ds}{dt} = \gamma np - \frac{s}{\tau_\mathrm{ct}} - k_\mathrm{d} s \,. \tag{S1b}$$

Making use of the same time harmonic representations for n, s, and J_r, along with the assumption that $n = p$, it is straightforward to derive their small-signal complex amplitudes:

$$\tilde{n} = \frac{\tilde{J}_\mathrm{r}}{qa[i\omega + 2\gamma n_0 - 2\gamma n_0 k_\mathrm{d}(i\omega + \tau_\mathrm{ct}^{-1} + k_\mathrm{d})^{-1}]}, \tag{S2a}$$

$$\tilde{s} = \frac{2\gamma n_0 \tilde{J}_\mathrm{r}}{qa[(i\omega + 2\gamma n_0)(i\omega + \tau_\mathrm{ct}^{-1} + k_\mathrm{d}) - 2\gamma n_0 k_\mathrm{d}]}, \tag{S2b}$$

that in turn lead to the MELS response, $\widetilde{M} = q\tilde{L}/\tilde{J}$, as described in the main text. Note, the DC carrier density in this case is the same as before, $n_0 = (J_{\mathrm{r}0}/qa\gamma)^{1/2}$. When k_d is small compared to both the electron-hole recombination rate ($\tau_\mathrm{rec}^{-1} = 2\gamma n_0$) and the natural CT state decay rate (τ_ct^{-1}), Equation (S2) yields the same result as Equation (4).

The existence of intersystem and reverse intersystem crossing (ISC and RISC, respectively) between singlet and triplet CT states can be treated in similar fashion. Assuming triplet CT states have a negligible natural decay rate, the differential equations in this case are:

$$\frac{dn}{dt} = \frac{dp}{dt} = \frac{J_\mathrm{r}}{qa} - \gamma np \,, \tag{S3a}$$

$$\frac{ds_\mathrm{S}}{dt} = \chi_\mathrm{S}\gamma np - \frac{s_\mathrm{S}}{\tau_\mathrm{ct}} - k_\mathrm{isc}s_\mathrm{S} + k_\mathrm{risc}s_\mathrm{T} \,, \tag{S3b}$$

$$\frac{ds_\mathrm{T}}{dt} = (1-\chi_\mathrm{S})\gamma np + k_\mathrm{isc}s_\mathrm{S} - k_\mathrm{risc}s_\mathrm{T} \,, \tag{S3c}$$

where s_S and s_T are the singlet and triplet CT state densities, χ_S is the fraction of electron-hole recombination events that form a singlet, and k_isc and k_risc are the intersystem and reverse intersystem crossing rates, respectively. Solving as above, the small signal charge density is the same as for Equation (1a) and the emissive singlet density is:

$$\tilde{s}_\mathrm{S} = \frac{2\gamma n_0 \tilde{J}_\mathrm{r}[\chi_\mathrm{S}(i\omega + k_\mathrm{risc}) + (1-\chi_\mathrm{S})k_\mathrm{risc}]}{qa(i\omega + 2\gamma n_0)[(i\omega + \tau_\mathrm{ct}^{-1} + k_\mathrm{isc})(i\omega + k_\mathrm{risc}) - k_\mathrm{isc}k_\mathrm{risc}]} \,. \tag{S4}$$

Although ISC and RISC is well-established in MTDATA:BPhen[32] and the photoluminescence transient in Section S2 below helps constrain the values of k_isc and k_risc, fits to the MELS data in Figure 2c,d are still not well constrained and therefore we opt to use the simplified model in the main text for the sake of transparency.

S2. Inhomogeneous broadening and the failure of quasi-equilibrium

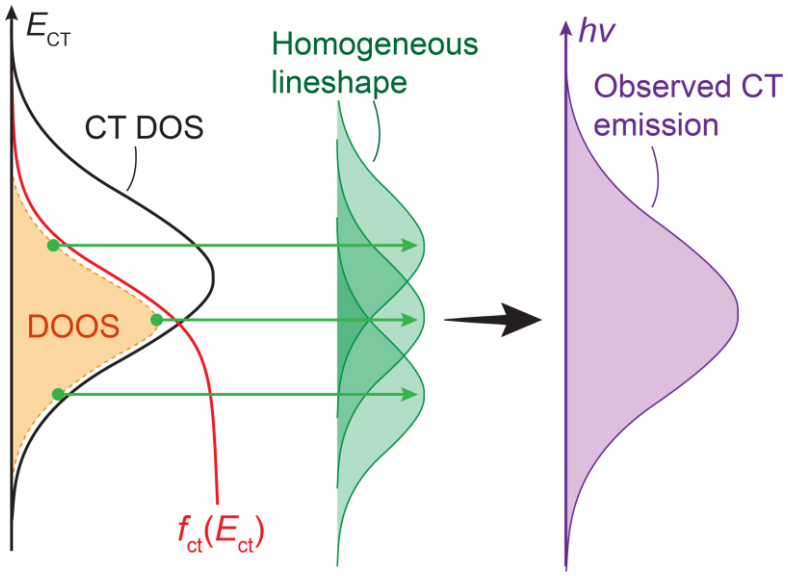

Figure S1. Illustration of a quasi-equilibrium picture of CT occupation, where the overlap of the CT occupation function ($f_{\mathrm{ct}}(E_{\mathrm{ct}})$) with the CT DOS yields the density of occupied CT states (DOOS). Radiative CT state decay at each energy leads to a homogeneously-broadened emission contribution that collectively lead to the observed CT emission spectrum. If inhomogeneous broadening (i.e. the width of the DOOS) were negligible, then the observed emission spectrum would exhibit the homogeneous linewidth and all photon energies would have the same MELS response since they originate from the same CT state, opposite to what is observed. Similarly, if the DOOS were in quasi-equilibrium, then modulating the voltage/current of the device would modulate the entire CT occupation function (e.g. by changing its chemical potential), causing CT states at all energies in the DOOS to respond in unison and thereby contribute emission with the same phase in the MELS spectrum. The observation of dispersive CT EL therefore confirms that inhomogeneous broadening is non-negligible, and that the CT DOOS does not exist in quasi-equilibrium.

S3. Transient photoluminescence

Figure S2a shows the spectrally-resolved CT PL transient recorded for a 1:1 MTDATA:BPhen film using a streak camera. The PL spectrum exhibits a dynamic red-shift over the first few μs (Figure S2b) along with a faster decay rate of the high energy spectral components as shown in Figure S2c. The bi-exponential form of the transient is consistent with that expected for ISC and RISC based on the solution of Equation S3b,c (without the generation terms[53]), and the lifetime of the longer-lived component is comparable to the value of τ_{ct} used to fit the MELS data in Figure 3.

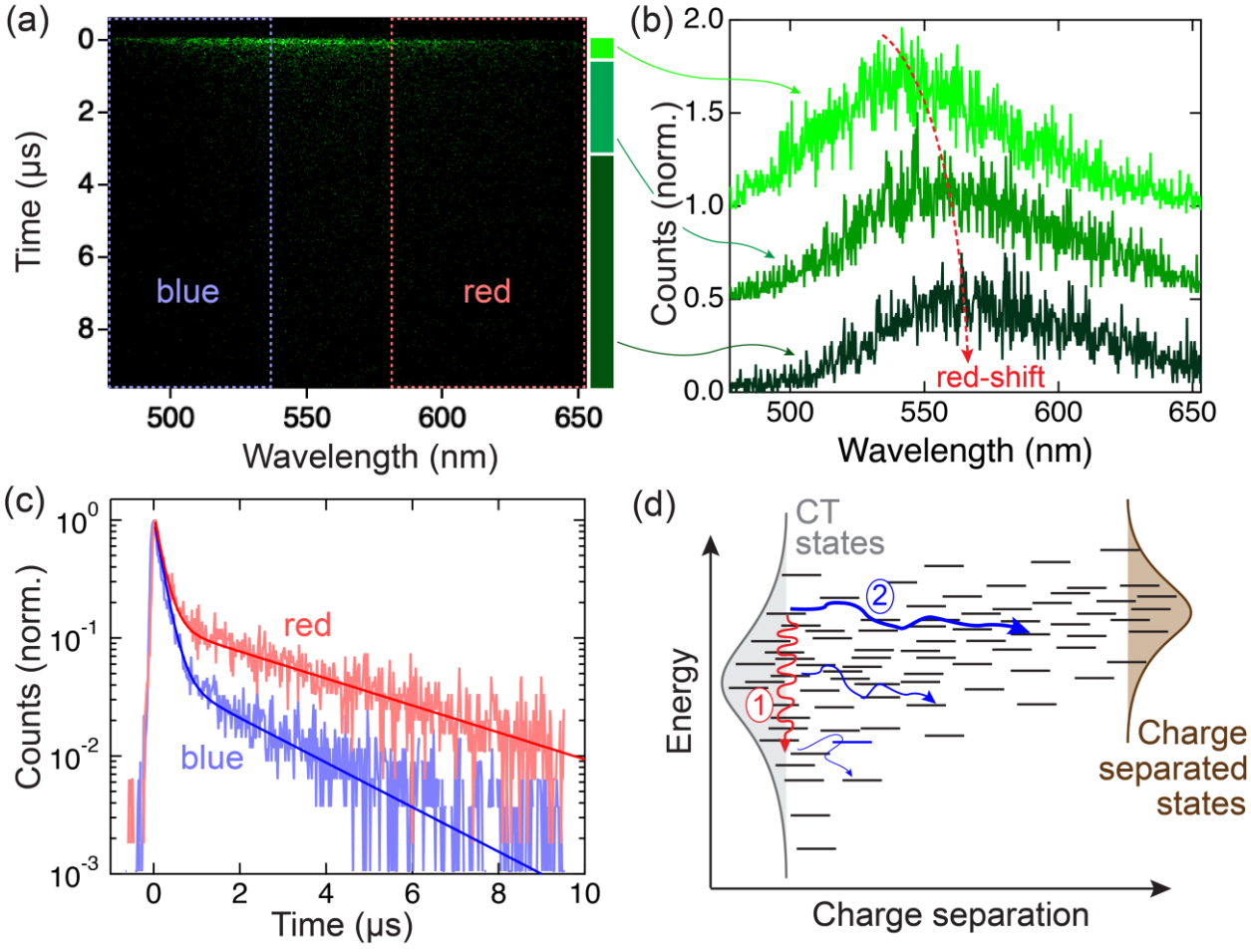

Figure S2. (a) Streak camera image of the PL transient of a 1:1 MTDATA:BPhen film deposited on a Si substrate. **(b)** Spectra integrated over different time intervals (green bars) in the streak image from panel (a). **(c)** Decay transient for the high (480-540 nm; blue) and low (580-650 nm; red) energy spectral components in the streak image. The dark solid lines are

biexponential fits to the data with lifetime components of 0.2 µs and 2.3 µs for the blue side of the spectrum and 0.2 µs and 3.8 µs for the red side. **(d)** Schematic showing two possible mechanisms that could lead to the dynamic red-shift and energy-dependent decay rate shown in (b) and (c). High energy CT states can relax geminately (i.e. the electron and hole remain bound throughout the process) via path 1, or they may dissociate faster than low energy CT states as indicated by path 2.

Figure S2b,c clearly demonstrates that high energy CT states in the DOS decay more rapidly than those at low energy. This could either be due to geminate CT state relaxation (path 1 in Figure S2d), energy-dependent CT state dissociation (path 2 in Figure S2d), or some combination of both. The former is known to occur in systems very similar to MTDATA:BPhen[16], and the latter is expected since high energy CT states have many lower energy hopping sites that can facilitate separation of the electron and hole[3,54].

S4. Summary of fit parameters

The parameters used to fit the data in Figure 2 and Figure 3 are summarized in Tables 1 and 2 below.

Table 1. Parameters used to fit the impedance and MELS data in Figure 2.

Current density (mA cm^{-2})	**0.01**	**0.1**	**1**	**4**
$\boldsymbol{\tau_{rec}}$ (µs)	226	53	6.7	2.6
$\boldsymbol{\tau_{ct}}$ (µs)	12	9	8	3.5
$\boldsymbol{R_s}$ (Ω cm^2)	120	120	120	120
$\boldsymbol{R_{rec}}$ (kΩ cm^2)	370	96	25	11

Table 2. Parameters used to fit the energy-dependent MELS data in Figure 3.

Filter wavelength (nm)	**488**	**510**	**540**	**580**	**640**	**710**
$\boldsymbol{\beta}$	0.79	0.89	1.02	1.1	1.13	1.13
$\boldsymbol{\tau_{rec}}$ (μs)	58	58	58	58	58	58
$\boldsymbol{\tau_{ct}}$ (μs)	4	4	4	4	4	4

S5. Planar heterojunction device data

Figure S3 shows the MELS spectra for a planar heterojunction (PHJ) device consisting of ITO/MTDATA (60 nm)/Bphen (60 nm)/LiF (0.5 nm)/Al (100 nm). The DC EL spectrum shown in the inset of Figure S3a is similar to that of the BHJ device shown in Figure 3a of the main text. Importantly, the PHJ MELS response is also dispersive and exhibits the same general trend with emission energy as observed for the BHJ case.

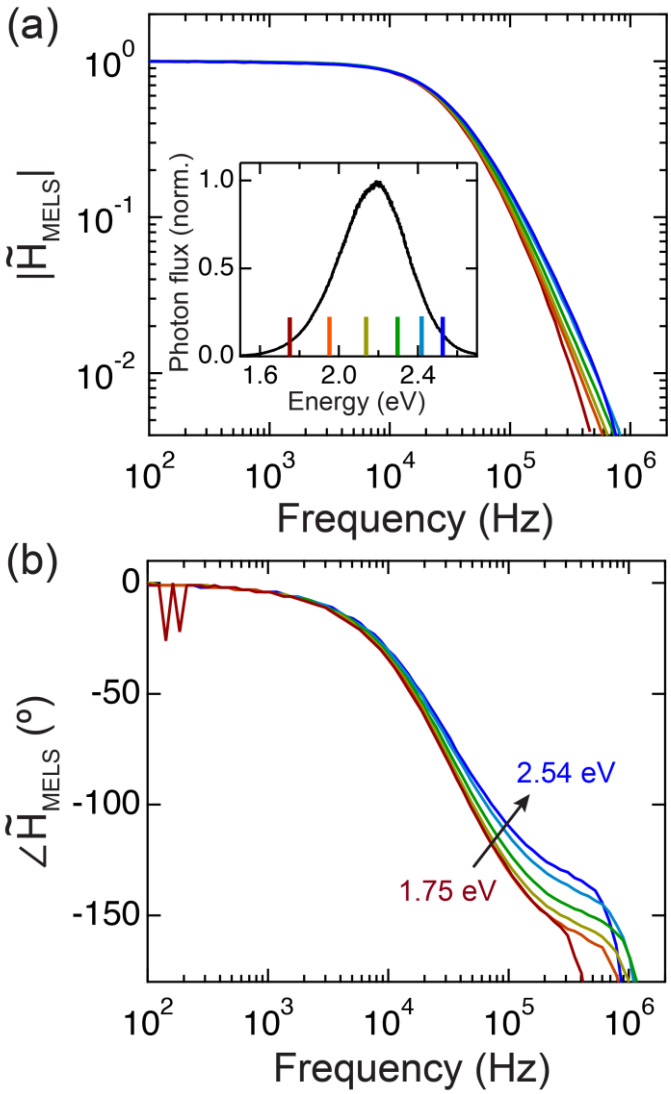

Figure S3. (a) Magnitude of the PHJ MELS response measured at different photon energies across the CT EL spectrum shown in the inset. The bias corresponds to a DC current density of 4 mA cm^{-2}. **(b)** Corresponding MELS phase response. The sharp fall-off in phase angle at high frequency is an artifact associated with low signal per the magnitude roll-off in (a).

S6. Cole-Davidson time constant distribution

As discussed in the main text, including a Cole-Davidson parameter, β, in the recombination term of the MELS transfer function implies a distribution of different recombination time

constants. Specifically, the Cole-Davidson pole in $\tilde{H}_{\mathrm{MELS}}$ given by $(1 + i\omega\tau_{\mathrm{rec}})^{-\beta}$ is associated with the distribution of time constants, τ, given by $f(\tau) = (\sin \pi\beta)/\left[\pi\tau(\tau_{\mathrm{rec}}/\tau - 1)^{\beta}\right]$ for $\tau < \tau_{\mathrm{rec}}$ and $f(\tau) = 0$ for $\tau > \tau_{\mathrm{rec}}$ [35,36]. As shown in Figure S4, this distribution function is very broad and weights toward smaller time constants as β decreases.

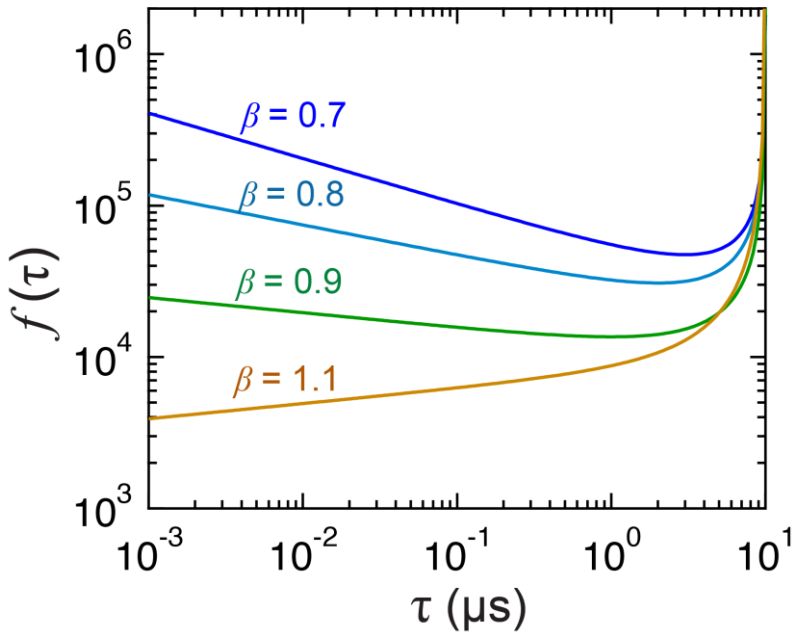

Figure S4. Distribution of time constants associated with the Cole-Davidson parameter, β, assuming a nominal recombination time constant, $\tau_{\mathrm{rec}} = 10$ μs.

Beyond simply reflecting that smaller β is indicative of a growing contribution of shorter time constant recombination processes, one should not attach too much meaning to the exact functional form of the distribution since there are other distribution functions that can yield a similar frequency response. However, as emphasized in Ref. [37], the statistical moments of the distribution expressed in terms of the logarithmic time constant, $\ln \tau$, are fairly unique for a given frequency response. Analytically, the average is $\langle \ln \tau \rangle = \ln \tau_{\mathrm{rec}} + \psi(\beta) + 0.58$, the variance is $\sigma^2_{\ln \tau} = \psi'(\beta) - \pi^2/6$, and the skewness is $\mu_{3\ \ln \tau} = \psi''(\beta) + 2.4$, where ψ, ψ', and ψ'' are the di-, tri-, and tetragamma functions, respectively. An added

advantage of working in terms of $\ln\tau$ is that, if the distribution of τ is associated with a distribution of activation energies, $G(E_\mathrm{a})$, where τ relates to E_a in Arrhenius fashion (i.e. $\tau = \tau_0 \exp(E_\mathrm{a}/k_\mathrm{b}T)$), then the moments above also yield the moments of the activation energy distribution[37], with the average given by $\langle E_\mathrm{a}\rangle = k_\mathrm{b}T(\langle\ln\tau\rangle - \ln\tau_0)$ and the standard deviation given by $\sigma_{\mathrm{E_a}} = k_\mathrm{b}T\sigma_{\ln\tau}$.

S7. Derivation of MELS model for energy-dependent recombination

Including the energy-dependent recombination rate given by Equation (5) in the MELS model from the main text leads to an energy-dependent version of Equation (1a) for the small-signal amplitudes given by:

$$\frac{d\tilde{n}(E_\mathrm{n})}{dt} = \frac{\tilde{J}_\mathrm{r}(E_\mathrm{n})}{qa} - \sum_{E_\mathrm{p}} \frac{q}{\varepsilon}\left[\mu_\mathrm{n}(E_\mathrm{n}) + \mu_\mathrm{p}(E_\mathrm{p})\right]\left[p_0(E_\mathrm{p})\tilde{n}(E_\mathrm{n}) + n_0(E_\mathrm{n})\tilde{p}(E_\mathrm{p})\right] \tag{S5a}$$

$$= \frac{\tilde{J}_\mathrm{r}(E_\mathrm{n})}{qa} - \sum_{E_\mathrm{p}} \frac{2\tilde{n}(E_\mathrm{n})}{\tau_\mathrm{n}(E_\mathrm{n}, E_\mathrm{p})},$$

Assuming symmetry between the electron and hole densities and mobilities as in Figure 5b, the right-hand bracketed term simplifies to $2p_0(E_\mathrm{p})\tilde{n}(E_\mathrm{n})$. The second equality in Equation (5a) subsequently makes use of $\tau_\mathrm{n}^{-1}(E_\mathrm{n}, E_\mathrm{p}) = (q/\varepsilon)\left[\mu_\mathrm{n}(E_\mathrm{n}) + \mu_\mathrm{p}(E_\mathrm{p})\right]p_0(E_\mathrm{p})$, which is the inverse lifetime of an electron at energy E_n due to recombination with holes at energy E_p. The energy-dependent version of Equation (1b) for the small signal CT state density is thus:

$$\frac{d\tilde{s}(E_\mathrm{ct})}{dt} = \sum_{E_n} \frac{2\tilde{n}(E_\mathrm{n})}{\tau_\mathrm{n}(E_\mathrm{n}, E_\mathrm{p})} - \frac{\tilde{s}(E_\mathrm{ct})}{\tau_\mathrm{ct}}. \tag{S5b}$$

Solving both equations in the frequency domain then yields:

$$\tilde{n}(E_\mathrm{n}) = \frac{\tilde{J}_\mathrm{r}(E_\mathrm{n})}{qa}\left[i\omega + \sum_{E_\mathrm{p}} \frac{2}{\tau_\mathrm{n}(E_\mathrm{n}, E_\mathrm{p})}\right]^{-1}, \tag{S6a}$$

$$\tilde{s}(E_{\mathrm{ct}}) \propto \frac{1}{(i\omega + \tau_{\mathrm{ct}}^{-1})} \sum_{E_{\mathrm{n}}} \frac{2\sigma_{\mathrm{n}}(E_{\mathrm{n}})}{\tau_{\mathrm{n}}(E_{\mathrm{n}}, E_{\mathrm{p}})} \left[i\omega + \sum_{E_{\mathrm{p}}} \frac{2}{\tau_{\mathrm{n}}(E_{\mathrm{n}}, E_{\mathrm{p}})} \right]^{-1}, \tag{S6b}$$

from which it is evident that there is a distribution of CT state formation time constants in Equation (S6b) – one for each bracketed term in the sum on E_{n}. The associated weights of each term are obtained by assuming that the energy-dependent electron recombination current distribution, $\tilde{J}_{\mathrm{r}}(E_{\mathrm{n}})$, is proportional to the energy-dependent electron conductivity, $\sigma_{\mathrm{n}}(E_{\mathrm{n}}) = q\mu_{\mathrm{n}}(E_{\mathrm{n}})n_0(E_{\mathrm{n}})$[41]. The net recombination rate of an electron at energy, E_{n}, with holes at all other energies, $E_{\mathrm{p}} = E_{\mathrm{n}} - E_{\mathrm{ct}} - E_{\mathrm{b}}$, is $\tau_{\mathrm{rec}}^{-1}(E_{\mathrm{n}}) = \sum_{E_{\mathrm{p}}} 2\tau_{\mathrm{n}}^{-1}(E_{\mathrm{n}}, E_{\mathrm{p}})$, where the factor of two results from the energetic symmetry of the electron and hole densities per Figure 5b. In simple language, Equation (S6a) reflects the net recombination rate of an electron at energy, E_{n}, with holes at all other energies, E_{p} (and vice versa due to the assumed symmetry of the problem), while Equation (S6b) reflects the formation of CT states from all of those recombination rates where $E_{\mathrm{n}} - E_{\mathrm{p}} = E_{\mathrm{ct}} + E_{\mathrm{b}}$.

The average of the distribution of logarithmic recombination time constants for all of these pathways that lead to CT state formation at E_{ct} is:

$$\langle \ln \tau_{\mathrm{rec}}(E_{\mathrm{ct}}) \rangle = \frac{\sum_{E_{\mathrm{n}}} w_{\mathrm{ct}}(E_{\mathrm{ct}}, E_{\mathrm{n}}) \ln(\tau_{\mathrm{rec}}(E_{\mathrm{n}}))}{\sum_{E_{\mathrm{n}}} w_{\mathrm{ct}}(E_{\mathrm{ct}}, E_{\mathrm{n}})}, \tag{S7}$$

where the weights in the summation, w_{ct}, are given by $w_{\mathrm{ct}}(E_{\mathrm{ct}}, E_{\mathrm{n}}) = \sigma_{\mathrm{n}}(E_{\mathrm{n}})\tau_{\mathrm{n}}^{-1}(E_{\mathrm{n}}, E_{\mathrm{p}})$ and the hole energy is related to the electron energy via $E_{\mathrm{p}} = E_{\mathrm{n}} - E_{\mathrm{ct}} - E_{\mathrm{b}}$. Because homogeneous broadening (with lineshape $g_{\mathrm{h}}(h\upsilon)$ given in the main text) mixes the response functions from multiple CT state energies at a given observed photon energy, $h\upsilon$, the experimentally-relevant MELS transfer function is obtained via discrete convolution: $\tilde{H}_{\mathrm{MELS}}(h\upsilon, \omega) \propto \tilde{s}(E_{\mathrm{ct}}) * g_{\mathrm{h}}(h\upsilon)$. The average logarithmic recombination lifetime at a given photon energy is therefore:

$$\langle \ln \tau_{\mathrm{rec}}(h\upsilon) \rangle = \frac{\sum_{E_{\mathrm{ct}}} \sum_{E_{\mathrm{n}}} w_{\mathrm{ct}}(E_{\mathrm{ct}}, E_{\mathrm{n}}) \ln\left(\tau_{\mathrm{rec}}(E_{\mathrm{n}})\right) g_{\mathrm{h}}(h\upsilon - E_{\mathrm{ct}})}{\sum_{E_{\mathrm{ct}}} \sum_{E_{\mathrm{n}}} w_{\mathrm{ct}}(E_{\mathrm{ct}}, E_{\mathrm{n}}) g_{\mathrm{h}}(h\upsilon - E_{\mathrm{ct}})}. \quad \text{(S8)}$$

The model is implemented assuming a Gaussian DOS for both holes and electrons given by $g_{\mathrm{n,p}}(E_{\mathrm{n,p}}) = N_{\mathrm{mol}}\left(2\pi\sigma_{\mathrm{n,p}}^2\right)^{-1/2} \exp\left[-\left(E_{\mathrm{n,p}} - E_{\mathrm{L,H}}\right)^2 / 2\sigma_{\mathrm{n,p}}^2\right]$, where N_{mol} is the molecular density, $E_{\mathrm{L,H}}$ are the LUMO and HOMO energies (Figure 5a), and $\sigma_{\mathrm{n,p}}$ are the corresponding standard deviations. Electron and hole occupation within each respective DOS is given by their corresponding Fermi-Dirac functions, $f_{\mathrm{n}}(E_{\mathrm{n}}) = (\exp((E_{\mathrm{n}} - E_{\mathrm{fn}})/k_{\mathrm{b}}T) + 1)^{-1}$ and $f_{\mathrm{p}}(E_{\mathrm{p}}) = 1 - \left(\exp\left(\left(E_{\mathrm{p}} - E_{\mathrm{fp}}\right)/k_{\mathrm{b}}T\right) + 1\right)^{-1}$, which depend on the electron and hole quasi-Fermi levels, E_{fn} and E_{fp}, as well as the thermal energy, $k_{\mathrm{b}}T$. Assuming that the resistive voltage drop is negligible, the quasi-Fermi level splitting (centered about mid gap due to the symmetry of the problem) is equal to the applied bias, $E_{\mathrm{fn}} - E_{\mathrm{fp}} = qV$. So long as the Boltzmann approximation holds ($V < 2$ V in this case), the DC CT EL spectrum is essentially independent of bias, though the corner frequency of the MELS spectrum does change due the associated variation in current density. Finally, the energy-dependent electron and hole mobility is calculated as described in Refs. [41,42] based on the hopping attempt frequency υ_0 and inverse wavefunction decay length α. Table 3 below summarizes the parameter values employed in this model to produce Figire 5b,c and Figure 6.

Table 3. Energy-dependent recombination model parameters used in Figure 5b,c and Figure 6.

Parameter	Symbol	Value
DOS parameters		
Molecular density (cm^{-3})	N_{mol}	10^{21}
DOS standard deviation (eV)	$\sigma_{\mathrm{n}} = \sigma_{\mathrm{p}}$	0.05
HOMO energy (eV)	E_{H}	0
LUMO energy (eV)	E_{L}	2.8
CT state binding energy (eV)	E_{B}	0.2
Mobility parameters		
Hopping attempt frequency (s^{-1})	υ_0	10^{11}
Inverse wavefunction decay length (nm^{-1})	α	0.5
Device parameters		
Recombination zone width (nm)	a	10
Relative dielectric constant	ε	3
Bias (V)	V	1.9
CT state parameters		
Reorganization energy (eV)	λ	0.3
CT state natural lifetime (μs)	τ_{ct}	10

S8. Fermi-Dirac approximation to non-equilibrium CT state distribution

Assuming that the CT state decay rate is energy-independent and that re-dissociation is negligible, the rate equation for the CT state density is:

$$\frac{ds(E_{\mathrm{ct}})}{dt} = K_{\mathrm{rec}}(E_{\mathrm{ct}}) - \frac{s(E_{\mathrm{ct}})}{\tau_{\mathrm{ct}}}. \tag{S9}$$

In steady-state, the density of occupied CT states within a small energy interval (dE_{ct}) centered about energy, E_{ct}, is therefore directly proportional to the electron-hole recombination rate from Equation (5):

$$s_0(E_{ct}) = \tau_{ct} K_{rec}(E_{ct}) dE_{ct} \,. \quad \text{(S10)}$$

Alternatively, the density of occupied CT states can be represented in terms of the CT DOS and a CT state occupation function, $f_{ct}(E_{ct})$, which for a quasi-equilibrium system, is just the Fermi-Dirac function (i.e. $f_{ct}(E_{ct}) = (\exp((E_{ct} - \mu_{ct})/k_b T) + 1)^{-1}$, where μ_{ct} is the CT state chemical potential[55]). Thus, from this this perspective, the CT state distribution is given by:

$$s_0(E_{ct}) = g_{ct}(E_{ct}) f_{ct}(E_{ct}) dE_{ct}. \quad \text{(S11)}$$

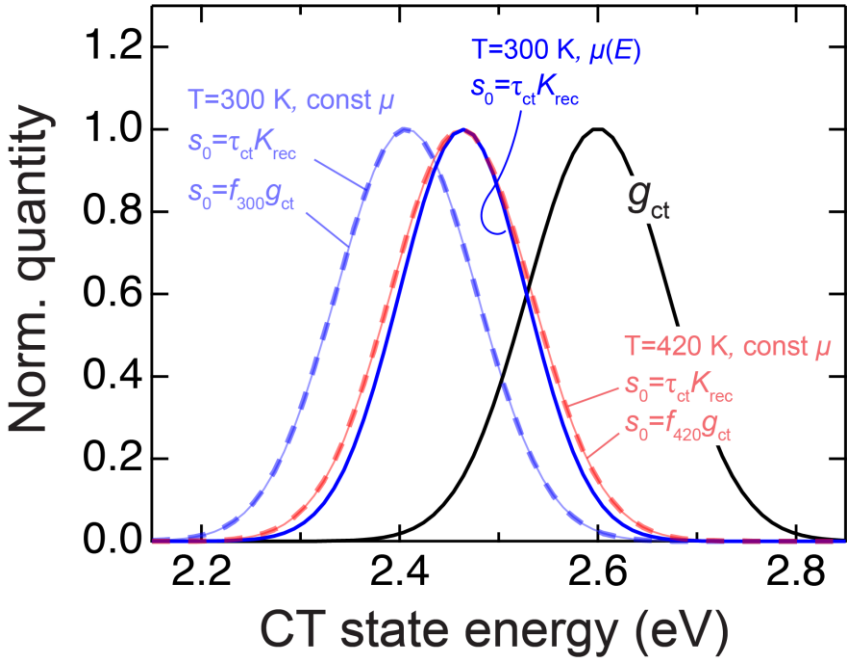

Figure S5. Normalized CT DOS (black line) together with the density of occupied states determined using Equation (S10) versus Equation (S11). Using constant mobilities, the kinetic- and occupation-determined distributions are the same at $T = 300$ K (light blue and dashed blue lines). However, in the energy-dependent mobility case, an effective temperature of $T = 420$ K is required for the peak of the occupation-based distribution (light red and dashed red lines) to match the peak of the $T = 300$ K kinetically-determined distribution (solid blue line).

Figure S5 shows that when the electron and hole mobilities used to calculate $K_{\mathrm{rec}}(E_{\mathrm{ct}})$ are constant (i.e. energy-independent), the kinetically-determined CT state distribution (Equation (S10)) is the same as that given by the occupation function-determined CT state distribution (Equation (S11)) as expected. When the electron and hole mobilities depend on energy as in Figure 5b, the peak of the kinetically-determined distribution shifts to higher energy (solid blue line). This shift can be approximated for the occupation function-determined distribution by using an elevated effective temperature of 420 K in f_{ct} (red lines), though the width of the distribution in this case is clearly too large. Thus, the CT state distribution associated with the energy-dependent Langevin coefficient in Equation (5) is not only non-thermal, but also non-equilibrium insofar as it cannot be described by the Fermi-Dirac form of f_{ct} using any effective temperature.

S9. Contribution of inhomogeneous broadening to the CT EL linewidth

In the model from Figure 5, the distribution of CT states (i.e. inhomogeneous broadening) accounts for roughly 12% of the emission linewidth. This is based on a homogeneous Gaussian full-width half-max (FWHM) linewidth of 0.295 eV (i.e. from Equation 6 based on $\lambda = 0.3$ eV and $k_{\mathrm{b}}T = 0.026$ eV in Table 3) and a ~0.15 eV FWHM of the calculated CT state distribution ($s_0(E_{\mathrm{ct}}) \propto K_{\mathrm{rec}}(E_{\mathrm{ct}})$ per Sec. S8 above), both of which are shown in Figure S6 below. The convolution of these functions gives the CT emission spectrum, $I_{\mathrm{em}}(h\nu)$ as described in the main text, which has a FWHM of 0.33 eV (comparable to the experimental FWHM linewidth of 0.37 eV in Figure 1b). The linewidth of the emission spectrum is therefore ~12% larger than it would be if homogenous broadening were the sole contribution.

We emphasize that, although this result is based on the use of representative material parameters in our model, the fractional contribution of inhomogeneous broadening is nevertheless tightly constrained by the amount of CT EL dispersion (e.g. degrees of phase

shift as a function of emission energy at a given modulation frequency). A substantially lower contribution (i.e. narrower $s_0(E_{ct})$) leads to no dispersion (red lines in Figure 6a,b), whereas a substantially higher contribution leads to more dispersion than is observed in Figure 3a,b. Hence, the ~1:2 *ratio* of inhomogeneous to homogeneous linewidth contributions (0.15 eV and 0.295 eV FWHM, respectively) that emerges from this model is probably close to the actual ratio for MTDATA:BPhen.

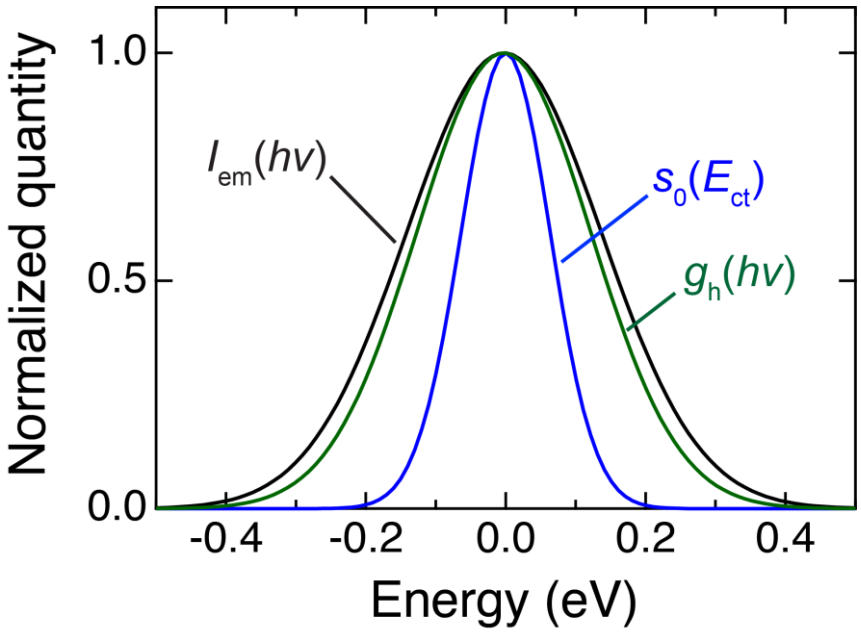

Figure S6. Normalized CT emission spectrum ($I_{em}(hv)$), distribution of occupied CT states ($s_0(E_{ct})$), and homogeneous linewidth ($g_h(hv)$, from Equation 6) based on the model from Figure 5 in the main text. The spectra have been centered to facilitate comparison of their linewidth.

References

[52] C. L. Braun, *J. Chem. Phys.* **1984**, *80*, 4157.

[53] N. A. Drigo, L. G. Kudriashova, S. Weissenseel, A. Sperlich, A. J. Huckaba, M. K. Nazeeruddin, V. Dyakonov, *J. Phys. Chem. C* **2018**, *122*, 22796.

[54] S. N. Hood, I. Kassal, *J. Phys. Chem. Lett.* **2016**, *7*, 4495.

[55] T. M. Burke, S. Sweetnam, K. Vandewal, M. D. McGehee, *Adv. Energy Mater.* **2015**, *5*, 1500123.